Characterization and the Effect of Different Parameters on Photocatalytic Activity of Montmorillonite/TiO$_2$ Nanocomposite under UVC Irradiation

Tam Thi Bang Dao[1,3], Loan Thi Thu Ha[1,3], Nhien Hon Le[1,3], Do Trung Nguyen[1,3], Truong Huu Nguyen[2,3], Chi-Nhan Ha-Thuc[1,3*]

[1] Faculty of Materials Science and Technology, University of Science, Ho Chi Minh City, Vietnam, 227 Nguyen Van Cu Street, Ward 4, District 5, Ho Chi Minh City 700000, Viet Nam
[2] Laboratory of Advanced Materials, University of Science, Ho Chi Minh City, Vietnam, 227 Nguyen Van Cu Street, Ward 4, District 5, Ho Chi Minh City 700000, Viet Nam
[3] Vietnam National University, Ho Chi Minh City, Vietnam, Linh Trung Ward, Thu Duc District, Ho Chi Minh City, 700000, Viet Nam
* Corresponding author, e-mail: htcnhan@hcmus.edu.vn

Abstract

This study aimed to modify montmorillonite (MMT) with titanium dioxide (TiO$_2$) by wet stirring method combined with ultrasonic to form MMT/TiO$_2$ nanocomposite and used as a photocatalyst in the removal of organic dye rhodamine B (RhB). The characteristics of the synthesized samples were analyzed by methods such as energy-dispersive X-ray spectroscopy (EDX), scanning electron microscope (SEM), transmission electron microscopy (TEM), X-ray diffraction (XRD), Fourier transform infrared spectroscopy (FTIR) and UV-Vis diffuse reflectance spectra (UV-Vis DRS). The degradation of RhB was carried out for 210 min under UVC irradiation, and the decolorization efficiency of RhB was evaluated by UV-vis spectroscopy. The results show that the TiO$_2$ anatase nanoparticles are randomly distributed on the surface or the space between the MMT sheets to form a house-of-card structure. After 210 min of exposure under a UVC light source, the decolorization efficiency reached 91.5% for the solution with pH = 6.8, photocatalyst content 0.1 g/L, initial concentration RhB 10 mg/L, and UVC power 15 W. Liquid chromatography–mass spectrometry (LCMS) identified the degradation intermediates that MMT/TiO$_2$ successfully cleaved the chromophore structure and formed more minor broken-ring by-products. The influence of operating parameters on RhB removal efficiency, including solution pH, photocatalyst content, initial dye concentration, inorganic, and organic scavengers, was studied. In addition, the kinetic modeling study shows that the RhB photodegradation reaction is consistent with the Langmuir-Hinshelwood first-order kinetic model.

Keywords

MMT/TiO$_2$ nanocomposite, photocatalyst, degradation, rhodamine B, organic dye, decolorization

1 Introduction

Titanium dioxide (TiO_2) is a potential metal oxide in photocatalysis. TiO_2 is a semiconductor of type $B^{IV}A^{VI}$ and can generate reactive radicals such as hydroxyl radicals $^{\cdot}OH$, superoxide anions $O_2^{\cdot-}$, and H_2O_2. In addition, TiO_2 exhibits many advantages over other photocatalysts due to its low cost, high photocatalytic efficiency, ease of preparation, and environmental friendliness. Therefore, TiO_2 is widely studied in environmental cleaning, and organic compounds' mineralization [1, 2]. The energy band characteristics of TiO_2 are wide bandgap energy (3.2 eV for anatase) and high-speed photogenerated electron-hole (e^--h^+)

recombination time [3, 4]. Therefore, to enhance the photocatalytic performance of TiO_2, many publications have demonstrated the effectiveness of modifying TiO_2 with different materials by different synthesis methods [5]. By supercritical antisolvent micronizing β-cyclodextrin (β-CD) and TiO_2 (PC500), Stefania Mottola et al. [6] create hybrid photocatalysts for UV light-driven degradation of azo dyes. The mineralization efficiency is 96% under UV irradiation [6]. Sridevi et al. [7] synthesised $TiO_2/BiOCl$ and $TiO_2/BiOCl/La_2O_3$ heterostructure photocatalyst by solid-state powder grind approach

for enhanced charge separation efficiency with improved UV-light catalytic activity towards rhodamine B (RhB) and Reactive Yellow 86 (RY). Degradation percentage was achieved between 95% and 92% for RhB and RY 86 dyes [7]. Zhengdong Zhang et al. [8] used a straightforward impregnation technique to create a novel Z-scheme $TiO_2/g-C_3N_4$ heterostructure photocatalyst to activate peroxymonosulfate (PMS) for the photocatalytic degradation of rhodamine B (RhB). Within 120 minutes of simulated sunlight exposure, the degradation rate of RhB (20 mg/L, 50 mL) was 82.79% [8]. Lan Zhang et al. [9] fabricated WO_3/TiO_2 membranes by reactive magnetron sputtering for rhodamine B dye degradation. The degradation percentage was 96.49% in 2 h under a 300 W mercury lamp irradiation [9]. However, along with the complex material synthesis process, the parameters affecting the photocatalytic efficiency and the by-products after photodegradation have not been investigated. Compared to previous studies, montmorillonit (MMT) was directly modified with anatase-phase TiO_2 powder, not from precursors of Ti such as tetraethyl orthotintanate (TEOT), titanium (IV) butoxide, etc. The method in this study allows the nanocomposite not to undergo thermal annealing and reduces chemical intermediates in the preparation process.

Based on our previous studies [10], MMT exhibits good swelling capacity, high ion exchange, and easy denaturation. MMT will exchange cations in the interlayer space of clay layers with inorganic polycations when combined with metal oxides. These polycations will be inserted into the interlayer space of clay. They convert to metal oxides when dried or heated by dehydrating and dehydroxylation. These metal oxides cluster together between clay layers and form a house-of-card structure. This structure is not only heat resistant but also maintains the distance between the clay layers and prevents the collapse of these layers. Due to the existence of empty areas between the layers, the clay becomes more porous. Thus, the emergence of a new porous structure and the enhancement of some active sites make this material more widely used in catalytic and adsorption activities. Our other recent study

showed that 0D TiO_2 (nanoparticles) and 1D TiO_2 (nanotubes) affected the RhB removal efficiency, namely, the efficiency of rhodamine B degradation under UVC light of MMT/TiO_2 is higher than that of MMT/TiO_2 nanotubes, and the adsorption process plays a vital role in the photodegradation process [11]. Accordingly, when MMT acts as the main phase in nanocomposites, the empty d orbitals of metal elements in the MMT trap the photogenerated electrons and prevent the recombination of the photogenerated electron-hole pairs (e^--h^+). This is considered a significant positive effect of MMT in the photocatalysis process. Besides, due to its excellent water swelling ability, MMT adsorbs organic dye molecules and forms active sites very well. Therefore, photo-oxidation and photo-reduction processes at valence and conduction bands of reactive radicals such as $^\cdot OH$, $O_2^{\cdot-}$, and H_2O will occur quickly [11–13]. In this paper, a comprehensive study on the operational parameters affecting the photocatalytic efficiency of MMT/TiO_2 nanocomposites was carried out, such as the pH value of dye solution, initial concentration dyes, photocatalyst content, inorganic and organic scavengers. Besides, the kinetic study and analysis of intermediate products after photocatalytic degradation time are clarified in this study.
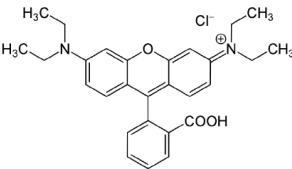
2 Materials and methods
2.1 Chemicals
All chemicals purchased from Merck Co., Germany, were of analytical grade and did not require further purification upon use, including anatase titanium dioxide (anatase TiO_2), ethanol, NaCl, KCl, KOH, HCl, NaH_2PO_4, $NaHCO_3$, Na_2SO_4, butanol, ethylenediaminetetraacetic acid (EDTA), and chloroform. Bentonite was purchased from Lam Dong, Vietnam. Rhodamine B was purchased from Sigma-Aldrich and had the characteristics described in Table 1.

2.2 Purification of montmorillonite from bentonite
The method of purifying MMT from bentonite is similar to our previous publications [10, 11] and is described according to Fig. 1. 200 g of bentonite is dispersed 24 h in 5 L

Table 1 Characteristics of Rhodamine B (RhB)

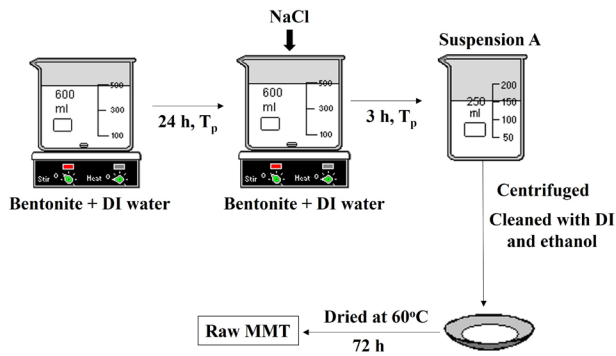| Index name, CAS number	Molecular formula	Chemical structure	λ_{max} (nm)	Class	M (g/mol)
C. I. Basic Violet 10, 81-88-9	$C_{28}H_{31}ClN_2O_3$		556	Azo	479.02

Fig. 1 Steps to synthesize montmorillonite (MMT) from bentonite

of deionized (DI) water and settled for 5 h. Add NaCl to the suspension mixture and stir for 3 h. Allow the mixture to settle for 24 h and centrifuge for 30 min. The obtained solid was washed several times with DI water, and ethanol. Finally, the suspension was centrifuged and dried at 60 °C for 72 h to obtain purified MMT.

2.3 Preparation of MMT/TiO$_2$ nanocomposite
Modifying MMT with TiO$_2$ to form MMT/TiO$_2$ nanocomposites is done similarly to our previously published method [11] and is described in Fig. 2. 2 g MMT was added to DI water and stirred for 24 h. Anatase nanoparticles were then added at a ratio of m_{MMT}:m_{TiO2} = 10:1. The mixture was stirred with a magnetic stirrer for 4 h, followed by ultrasonication for 1 h. Finally, the mixture was centrifuged and dried at 80 °C for 24 h to obtain MMT/TiO$_2$ nanocomposite.

2.4 Characterization
Energy dispersive X-ray spectroscopy (HORIBA H-7593 EDX, Horiba, England) was carried out to determine the elemental composition of MMT and MMT/TiO$_2$. Scanning electron microscopy (Hitachi S4800, Japan), and transmission electron microscopy (JEOL JEM-1400,
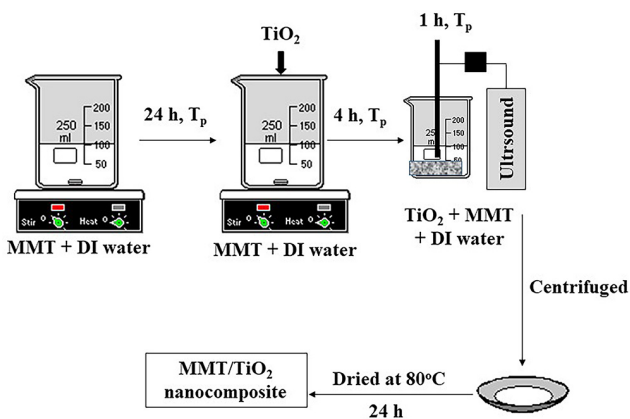

Fig. 2 Steps to synthesize MMT/TiO$_2$ nanocomposite

USA) were used to observe the surface morphology and particle size of MMT and MMT/TiO$_2$. X-ray diffraction (D2 PHASER XRD, Bruker, Germany) was used to determine the crystal characteristics of TiO$_2$, MMT, and MMT/TiO$_2$. The radiation source was Ni-filtered CuK with λ = 0.15406 nm. The applied current and voltage were 40 mA and 40 kV with a scan rate of 0.030°/s 2θ = 5–80°. The average crystal size in this study was calculated according to the Scherrer formula Eq. (1):

$$D = \frac{k\lambda}{B\cos\theta} \tag{1}$$

where D: the average size of the particle (nm); θ: the Bragg angle (°); B: full width at half maximum (FWHM) of the diffraction peak (rad); λ: the X-ray wavelength (λ = 1.5406 Å); k: the shape factor (k = 0.9).

The bonding vibrations of TiO$_2$, MMT, and MMT/TiO$_2$ in the range from 4000 to 400 cm^{-1} were analyzed by Nicolet iS 50 FTIR (Thermo, USA). The bandgap energies E_g of TiO$_2$, MMT, and MMT/TiO$_2$ were measured by absorption spectroscopy UV-Vis DRS (V-770 UV-VIS-NIR Spectrophotometer JASCO Inc., Japan) and calculated from the Tauc plot by plotting the correlation between the photo-light power and $(\alpha h v)^{1/2}$. The intermediate products of RhB degradation were analyzed with LC-MS (m/z = 30–600) in positive ion mode and a gas flow rate 800 L/h.

The pH value at which the surface charge equals zero under certain temperature, pressure, and aqueous solution component conditions is referred to the point of zero charge pH_{pzc}. If pH < pH_{pzc}, the surface is positively charged and negatively charged otherwise. The pH_{pzc} of MMT/TiO$_2$ was determined as follows: 10 mg of MMT/TiO$_2$ was added to the 0.1 M KCl solution, and the pH of KCl solution was adjusted from 2 to 12 (pH_i) with 0.1 M KOH or 0.1 M HCl. After the solution reached equilibrium, the pH of the solution was re-determined and called pH_f. From there, determine the value $\Delta pH = pH_f - pH_i$. Plot ΔpH against pH_i; the value at which the line intersects the Ox axis is called the pH_{pzc} of the material [14–17]. The Ox axis is horizontal, perpendicular, and passes through the origin O (0; 0).

2.5 Decolorization setup
The photocatalytic degradation process of rhodamine B was carried according to Fig. 3 [11]. Photocatalytic tests were performed in a closed chamber with a 15 W UVC lamp positioned 10 cm above the solution surface. 10 mg of the photocatalyst was added to 100 mL of RhB solution
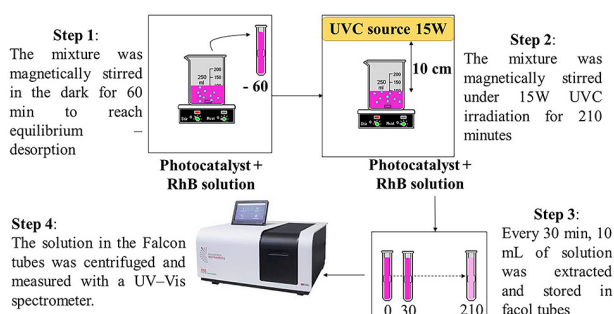
Fig. 3 Procedure for decolorization of RhB solution

and stirred with a magnetic stirrer for 60 min to reach adsorption-desorption equilibrium. Then, the UVC lamp was turned on for 210 min to initiate the photocatalysis. During this time, every 30 minutes, 5 mL of solution was extracted and centrifuged for UV-Vis spectroscopy to assess the change in concentration over time. The efficiency of the decolorization process is determined by the formula Eq. (2):

$$\text{Decolorization efficiency } (\%) = \left[\frac{C_0 - C}{C_0} \right] \times 100 \qquad (2)$$

where C_0: the concentration of the RhB initially (mg/L). C: the concentration of the RhB at time t (mg/L).

3 Results and discussion
3.1 Characterization of the synthesized MMT/TiO$_2$ nanocomposite

The surface morphology and particle size were observed by TEM and SEM images as shown in Figs. 4 and 5. MMT sheets with flake shapes have diameters from 480 to 1000 nm respectively (Fig. 4 (a) and Fig. 4 (b)). These sheets are distributed according to the layered structure observed on the MMT surface (Fig. 5 (a)). The anatase nanoparticles (Merck) have a spherical shape and average size of 70–150 nm (Fig. 4 (c) and Fig. 4 (d)). TiO$_2$ nanoparticles are not distributed discretely but in clusters. When TiO$_2$ was dispersed into the MMT by ultrasound, the TiO$_2$ nanoparticles in the nanocomposite were smaller in size than that of the raw TiO$_2$ (Fig. 4 (e) and Fig. 4 (f)). SEM images (Fig. 5 (b)) and TEM images (Fig. 4 (e) and Fig. 4 (f)) show that TiO$_2$ nanoparticles are randomly and heterogeneously distributed on the surface or in the space between the MMT sheets [11, 18, 19]. Fig. 6 is the EDX spectrum of MMT and MMT/TiO$_2$. The composition of MMT includes K, Na, Al, Ca, O, Si, Fe, and Mg. The elemental composition of the nanocomposite MMT/TiO$_2$ includes elements similar to that of MMT and Ti

with a minimum of 1.91 wt%. This indicates the presence of Ti and the elements of MMT in the MMT/TiO$_2$ nanocomposite [11, 20–22].

X-ray diffraction patterns of TiO$_2$, MMT, and MMT/TiO$_2$ are shown in Fig. 7. TiO$_2$ nanoparticles have diffraction characteristics of the anatase phase (JCPDS No. 21-1272), including reflection planes: (101), (103), (004), (112), (200), (105), (211), (204), (116), (220), and (215). The average crystal size of TiO$_2$ calculated from the Scherrer formula (Eq. (1)) is about 0.3 nm. This result is similar to that of Gao K. Zhang et al. [23]. MMT, after being purified from bentonite, has a (001) reflection plane at $2\theta = 25.2°$, and the basal spacing of (001) calculated based on the FMHW value from Origin software is about 14.5 Å, equivalent to many previous publications [24, 25]. It is noteworthy that the (001) pak of MMT has shifted slightly toward the higher 2θ angle, and the basal spacing of (001) is reduced to 14.0 Å when the MMT is modified with TiO$_2$ nanoparticles. This showed that TiO$_2$ nanoparticles were intercalated in the clay sheets and reduced the distance between the clay layers, forming a house-of-card structure [26]. The intensity of the reflection plane at $2\theta = 25.2°$ is enhanced compared with that of the raw MMT, indicating a contribution from the reflection plane (101) anatase to the structure of the nanocomposite. Because the content of TiO$_2$ is slow, the diffraction pattern of MMT/TiO$_2$ almost only contains the diffraction peaks of MMT.

Fig. 8 shows the FTIR spectra of TiO$_2$, MMT, and MMT/TiO$_2$. TiO$_2$ has only one absorption region at 430 cm^{-1}, which is attributed to Ti–O stretching vibration [16]. The FTIR spectra of the MMT show many absorption bands. The absorption bands at 3620 and 3420 cm^{-1} are attributed to the –OH asymmetric stretching and symmetrical stretching vibrations of the H$_2$O molecules interwoven into the MMT structure. Meanwhile, the absorption band at 1640 cm^{-1} is attributed to the interlayer H–O–H stretching vibration. The absorption bands at 1050 and 784 cm^{-1} are attributed to the Si–O asymmetric stretching vibration and the Al–O stretching vibration, respectively. The stretching Al–O–Si and strain Si–O–Si vibrations represent the wavenumbers at 530 and 462 cm^{-1} [27, 28]. The amount of TiO$_2$ is too small to make a difference in the absorption bands of the MMT/TiO$_2$ compared to that of the MMT due to the overlap between the vibration bands. Ti–OH and Ti–O–Ti stretching vibration will appear at the absorption band 1638 and 1571 cm^{-1}, respectively; Ti··O–Si stretching vibration will appear at the absorption band 915 cm^{-1} [28–30].
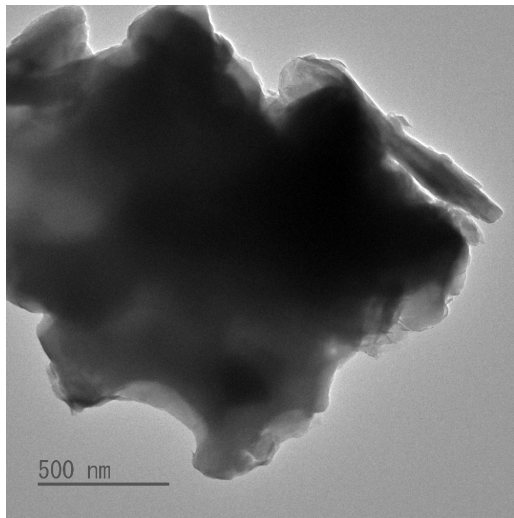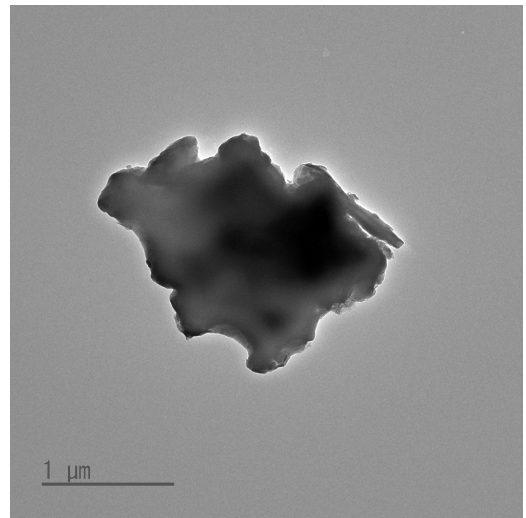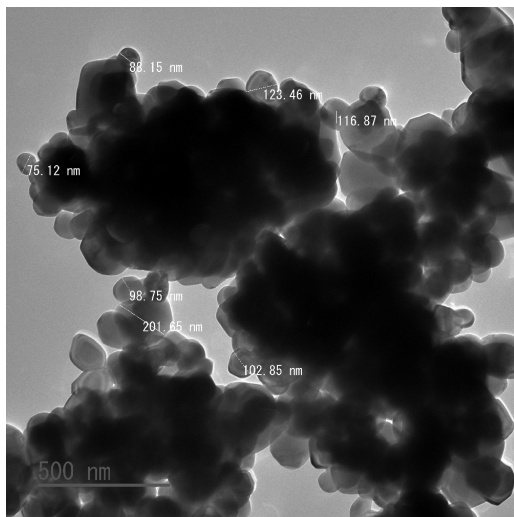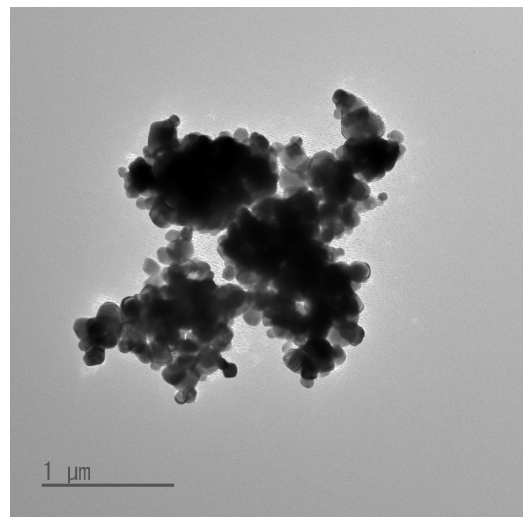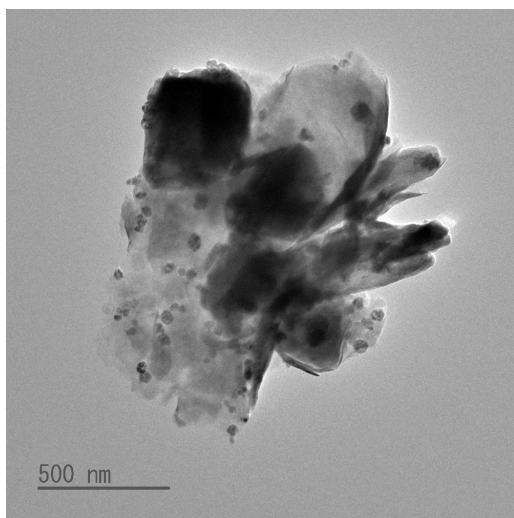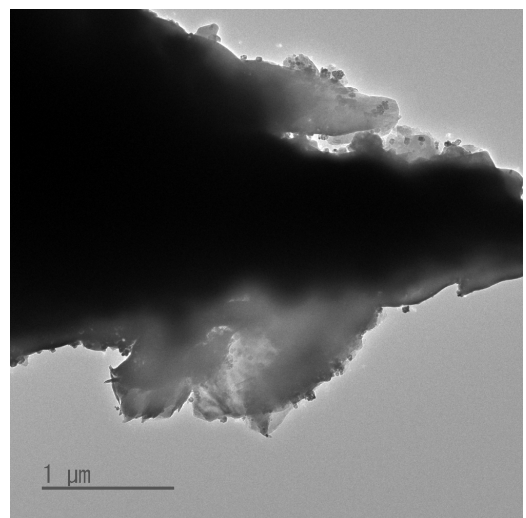
Fig. 4 TEM images of MMT at various magnifications: (a) 500 nm, (b) 1 μm; TEM images of TiO$_2$ at various magnifications: (c) 500 nm, (d) 1 μm; and TEM images of MMT/TiO$_2$ at various magnifications: (e) 500 nm, (f) 1 μm
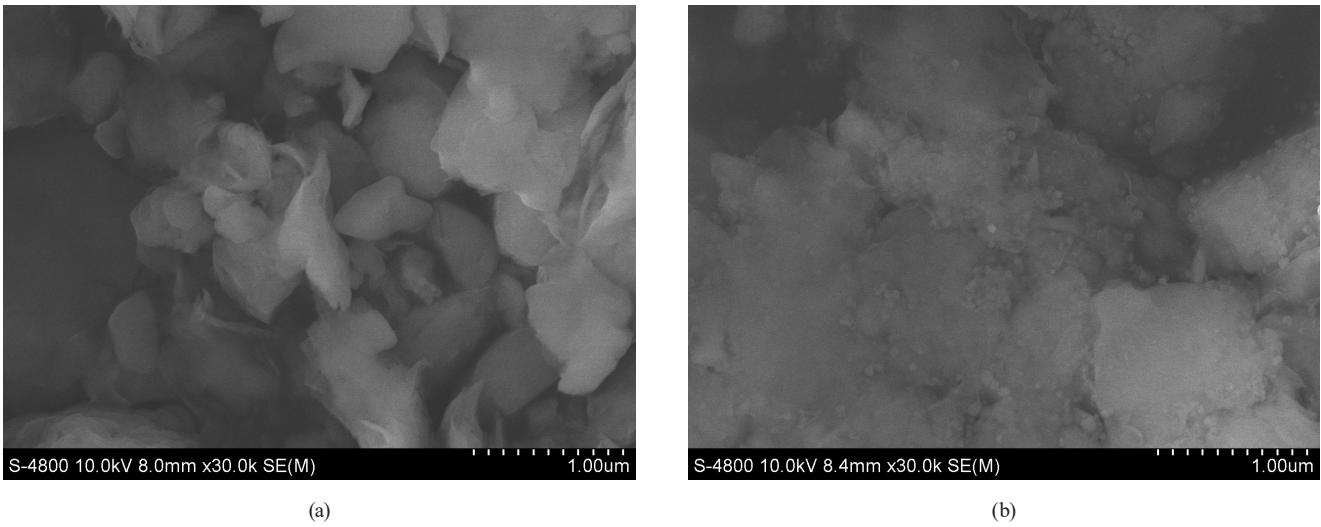
(a)   (b)

Fig. 5 SEM images of (a) MMT powder, and (b) MMT/TiO$_2$ nanocomposite
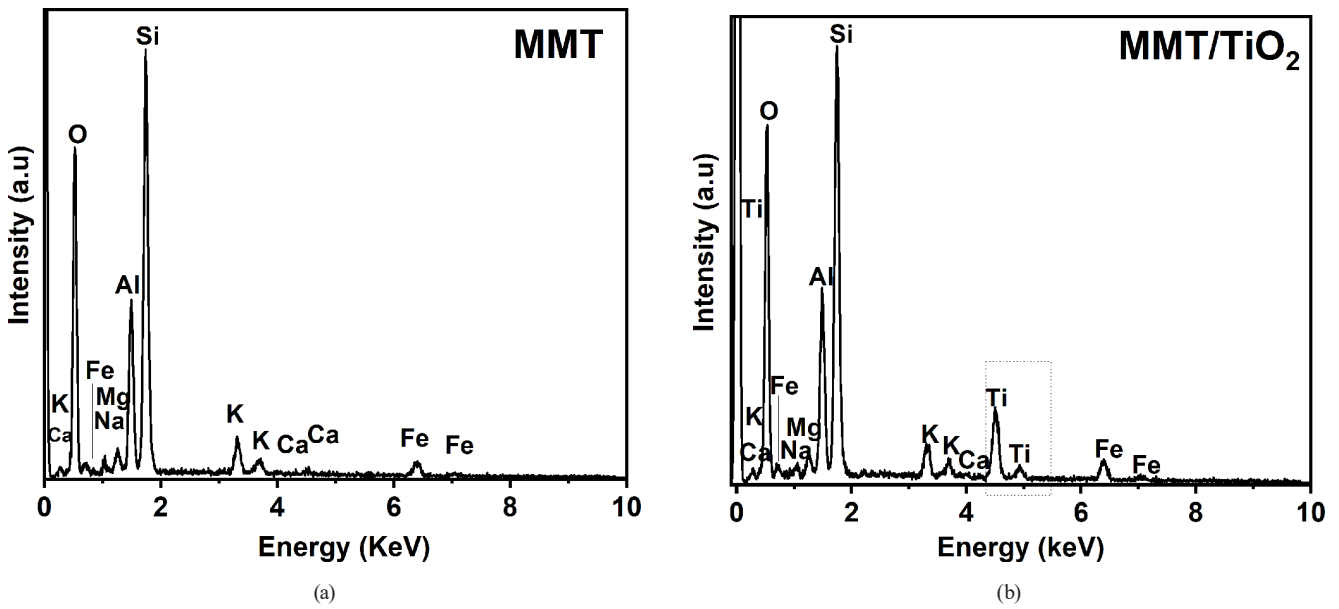

(a)   (b)
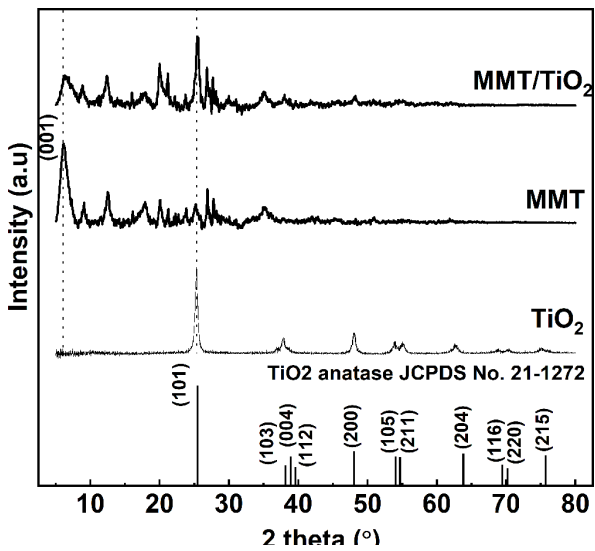
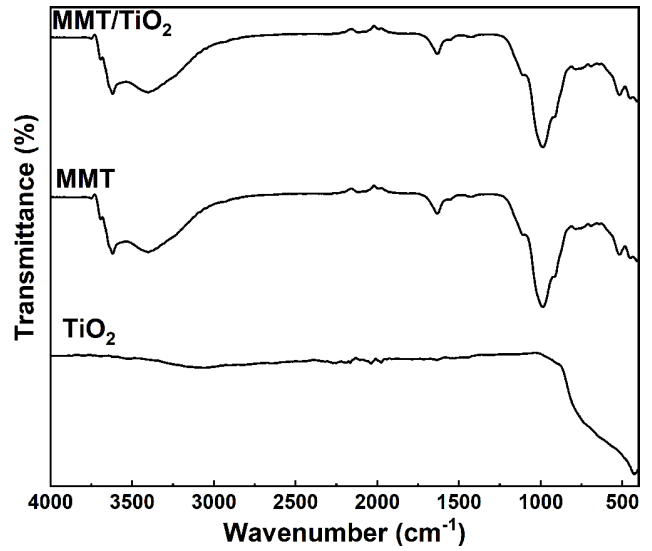**Fig. 6** EDX spectra of (a) MMT and (b) MMT/TiO$_2$

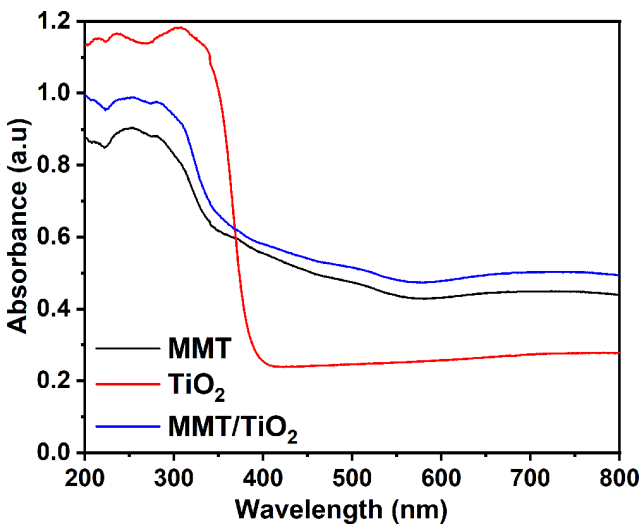**Fig. 7** XRD patterns of TiO$_2$, MMT and MMT/TiO$_2$

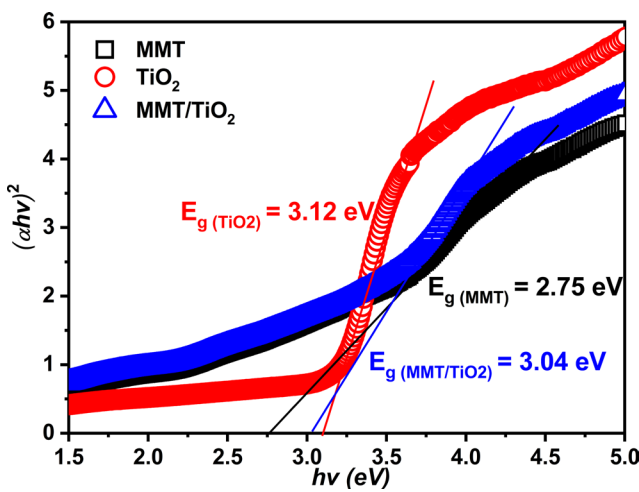**Fig. 8** FTIR spectra of TiO$_2$, MMT, and MMT/TiO$_2$

Fig. 9 (a) depicts the UV-Vis DRS spectra of MMT, TiO_2, and MMT/TiO_2. The absorption edges of MMT, TiO_2, and MMT/TiO_2 appeared at 310 nm, 365 nm, and 320 nm, respectively. It was found that the absorption edge of MMT/TiO_2 has a slight shift to the visible region due to the influence of a small amount of TiO_2 immobilized in the nanocomposite. The band gap energies of MMT, TiO_2, and MMT/TiO_2 were determined by the Tauc formula Eq. (3) [31, 32]:

$$\alpha h v = C \left(h v - E_g \right)^m , \qquad (3)$$

where h: the Planck constant; v: the photon frequency; E_g: the band gap energy (eV); α: the adsorption coefficient; C is a constant; m: factor depends on the nature of the electron transition and is equal to 1/2 or 2 for the direct and indirect transition band gaps, respectively.

TiO_2 is an indirect band gap semiconductor, so the band gap energies were evaluated according to the plot of $(\alpha h v)^2$ versus photon energy (eV) (Fig. 9 (b)). The estimated band gap energy values for the MMT, TiO_2, and MMT/TiO_2 were 2.75, 3.12, and 3.04 eV, respectively. Compared with TiO_2 (E_g = 3.12 eV), the band gap energy of MMT/TiO_2 has been narrowed to 3.04 eV. This result is consistent with the results reported in the literature [33–35]. Previous studies determined that the absorption edge shifts to a shorter wavelength when the TiO_2 content in the composites is low and the grain size of TiO_2 is as small as nm. Accordingly, the quantum size effect is responsible for the blue shift of the band edge, namely that the TiO_2 nanoparticles intercalated on MMT were small enough to show the quantum size effect [34, 35].

3.2 Effect of operational parameters on the decolorization performance of Rhodamine B

3.2.1 Effect of pH values

The value of pH$_{pzc}$ may vary depending on the method of preparation or the ratio of components in the composite. Indeed, previous publications showed that with the same hydrothermal method, Alireza Khataee et al. [36] revealed the pH$_{pzc}$ of MMT/TiO_2 to be 6.8, while Aydin Hassani et al. [14] revealed the pH$_{pzc}$ of MMT/TiO to be 8.4. Fig. 10 shows the point of zero charge of the MMT/TiO_2 nanocomposite in this study. The results show that MMT/TiO_2 has a pH$_{pzc}$ = 6.5. Therefore, when MMT/TiO_2 is investigated in an environment with pH > 6.5, the material will be negatively charged and generate electrostatic attraction with positively charged RhB molecules. At that time, RhB molecules are readily adsorbed on the MMT/TiO_2 surface and vice versa in environmental conditions
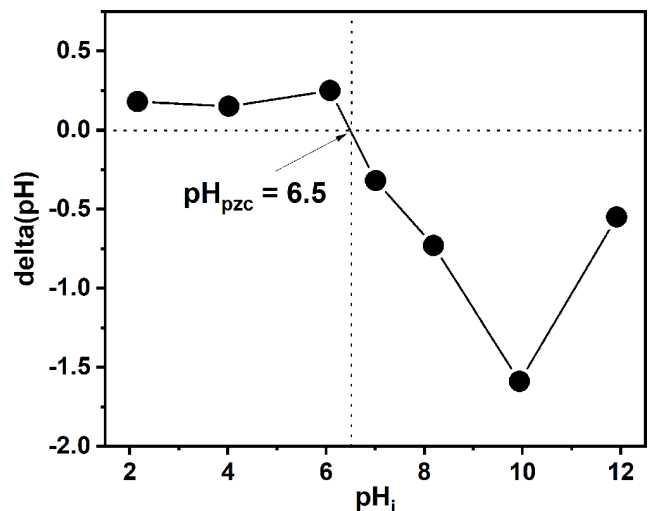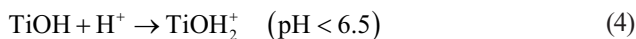

(a)

(b)

Fig. 9 (a) UV-Vis DRS spectra of MMT, TiO_2, and MMT/TiO_2; (b) Kubelka-Munk function versus the photon energy.

Fig. 10 Point of zero charge (pH$_{pzc}$) of MMT/TiO_2

with pH < 6.5 [15, 16]. The surface ionization state of TiO_2 is affected by the pH in the medium according to the Eq. (4) and Eq. (5):

$$TiOH + H^+ \rightarrow TiOH_2^+ \quad (pH < 6.5) \tag{4}$$

$$TiOH + OH^- \rightarrow TiO^- + H_2O \quad (pH > 6.5). \tag{5}$$

The pH of the solution is one of the critical factors affecting the decomposition efficiency of many organic substances in the photocatalysis process. Based on the point of zero charge of MMT/TiO_2, the photodegradation efficiency of RhB was experimented with at different pH values from 5 to 10 and presented in Fig. 11. Without any adjustments, the dye solution had a pH of 6.8. The decolorization efficiency H% at the various pH values decreases in order: $H\%_{pH6.8} > H\%_{pH8} > H\%_{pH5} > H\%_{pH10}$. The effect of pH on photocatalytic degradation depends on factors such as electrostatic interactions between the photocatalyst surface, solvent molecules, colored molecules, and charged radicals formed during the photocatalysis reaction process. RhB is an azo-colored organic dye (−N = N) that exists as a cation in an aqueous medium with an acid dissociation constant pKa = 3.7. That is, when pH > 3.7, the surface of the RhB molecule is positively charged [37]. When $pKa < pH = 5 < pH_{pzc}$, the MMT/TiO_2 surface has a positive charge due to protonation, while the RhB molecule also has a positive charge, so the interaction between the photocatalyst surface and RhB is mainly the electrostatic repulsion of positive charges, leading to reduced RhB adsorption on the catalyst surface and low decolorization efficiency ($H\%_{pH5} = 72.8\%$). Moreover, the positive
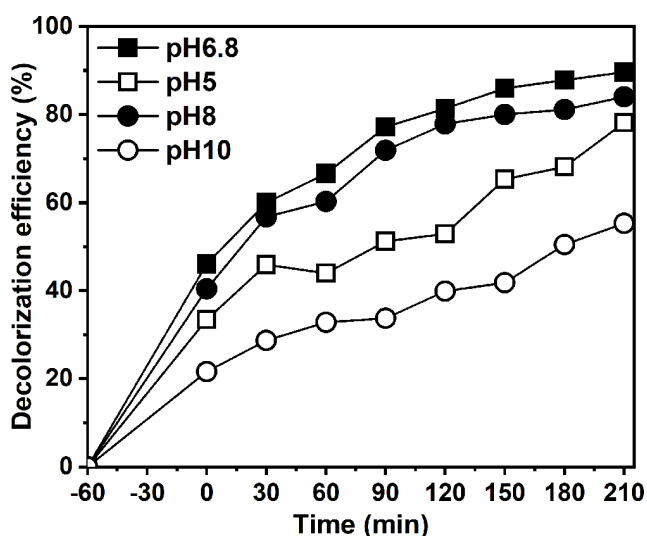
charge on the surface of MMT/TiO_2 limits the hydroxyl ions required for forming free radicals, which plays an essential role in the degradation of color compounds. In contrast, when $pKa < pH_{pzc} < pH = 6.8$, the photochemical degradation efficiency increased sharply due to the electrostatic interaction between the RhB cation and the negatively charged MMT/TiO_2 surface from proton separation, which increased the adsorption capacity and helped the photocatalytic reaction more efficiently ($H\%_{pH6.8} = 91.5\%$). The reason for the increase in decolorization efficiency when increasing the pH value is also due to the rise in the number of hydroxyl ions at the surface of the photocatalyst, leading to the formation of many hydroxyl radicals according to Eq. (6) [38]:

$$h^+ + OH^- \rightarrow OH^\bullet. \tag{6}$$

However, the decolorization efficiency decreased gradually in an alkaline medium ($H\%_{pH8} = 83.7\%$) and fell sharply when the pH of the solution was 10 ($H\%_{pH10} = 56.2\%$). The higher the pH of the solution, the more negatively charged the MMT/TiO_2 surface. A large number of positively charged RhB molecules will be adsorbed on the MMT/TiO_2 surface, leading to the RhB molecules becoming agents to prevent UVC from reaching the TiO_2 energy region. This reduces the photocatalytic efficiency [38]. Opposite, more decrease in the pH of the solution led to an increase in coulombic repulsion between the positively charged MMT/TiO_2 surface and RhB molecules, leading decrease in the decolorization efficiency [14, 16]. It is confirmed that adsorption is essential in the photocatalysis of MMT/TiO_2 nanocomposites [16, 39]. Therefore, other experiments in this study were performed with pH 6.8.

3.2.2 Effect of photocatalyst dosages

MMT/TiO_2 with different concentrations: 0.05; 0.1; 0.15; 0.2, and 0.3 g/L were added to 100 mL of 10 mg/L RhB solution and pH = 6.8, respectively. The mixture was adsorbed for 60 minutes, and UVC irradiated for 210 minutes afterward. The results illustrated in Fig. 12 show that the RhB removal efficiency increased from 81.8 to 96.2%, corresponding to an increase in the amount of MMT/TiO_2 catalyst from 0.05 to 0.2 g/L. Indeed, when the amount of photocatalyst is low, the total surface area exposed to RhB is less, leading to a decrease in the active degradation sites and a decrease in the decolorization efficiency. On the contrary, the reaction sites will increase with the increase of photocatalyst, resulting in more hydroxyl radicals being generated and increasing the photocatalytic
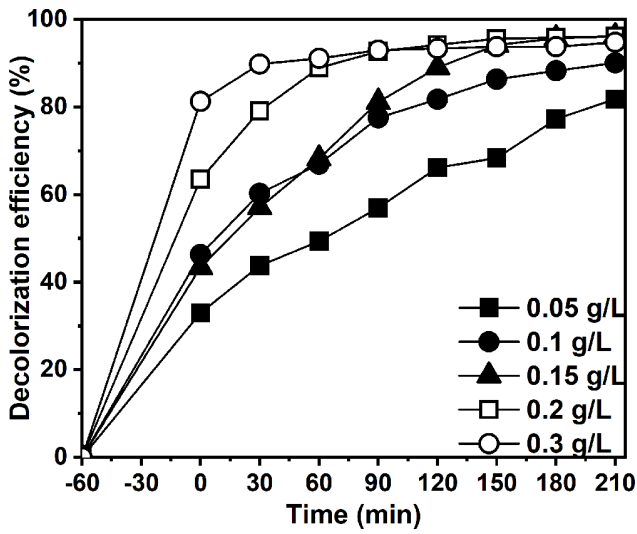

Fig. 11 Effect of initial pH on the photocatalytic of RhB under UVC 15 W ($m_{MMT/TiO2} = 0.1$ g/L and $C_0 = 10$ mg/L)

Fig. 12 Effect of the MMT/TiO$_2$ dosages on the photocatalytic of RhB under UVC 15 W (C_0 = 10 mg/L and pH = 6.8)

Fig. 13 Effect of initial RhB concentration on the photocatalytic of RhB under UVC 15 W ($m_{MMT/TiO2}$ = 0.1 g/L and pH = 6.8)

activity. However, when the amount of photocatalyst in the solution increases too much, the disorder in the solution also increases. This will limit the path of light and reduce irradiation. As a result, although the amount of catalyst increased significantly, the RhB degradation efficiency decreased, which is in good agreement with other studies [40, 41].

3.2.3 Effect of initial Rhodamine B concentration
The influence of the initial dye concentration is an essential parameter of most photochemical degradation processes. Experiments were performed by gradually increasing the initial concentration of RhB from 3 mg/L to 20 mg/L while keeping the amount of photocatalyst at 0.1 g/L and the pH of the solution fixed at 6.8. The results illustrated in Fig. 13 show that the RhB removal efficiency decreased from 99.9% to 52.5%, corresponding to an increase in the initial RhB concentration from 3 to 20 mg/L. The photodegradation rate is related to the formation of the •OH radical on the photocatalyst surface and the possible reactivity between the •OH radical and the colored molecules. When the initial RhB concentration increased, many RhB molecules were adsorbed at the surfactant sites of the MMT/TiO$_2$ photocatalyst, leading to a decrease in the adsorption of hydroxyl ions (OH$^-$) at these sites [14–16]. That is, the rate of formation of hydroxyl radicals – the primary oxidizing agent necessary for increasing photodegradation efficiency – decreases accordingly. On the other hand, according to the Beer-Lambert law, as the concentration of the colored substance increases, the distance of photons entering the solution decreases. Therefore, the

photons can be intercepted before reaching the photocatalyst surface and reduce the photon absorption, leading to a decrease in photodegradation [42–44].

3.2.4 Effect of inorganic and organic scavengers
The dye removal efficiency is affected by a large amount of inorganic and organic ions usually present in the wastewater. This paper added 0.05 g/L of NaCl, NaH$_2$PO$_4$, NaHCO$_3$, and Na$_2$SO$_4$ to 100 mL of a solution containing RhB 10 mg/L and 0.1 g/L MMT/TiO$_2$, respectively, to investigate the influence of inorganic salt ions on the decomposition of RhB. As observed from Fig. 14, the RhB decolorization efficiency of MMT/TiO$_2$ in the presence of inorganic ions, including chloride (Cl$^-$), dihydrogen
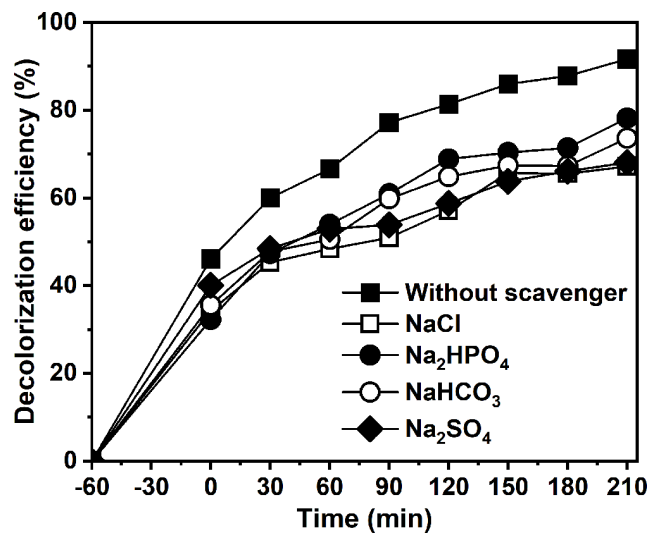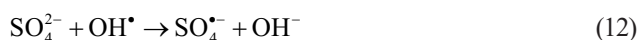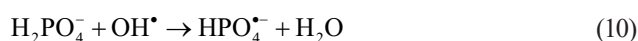

Fig. 14 Effect of inorganic scavengers on the photocatalytic of RhB under UVC 15 W ($m_{MMT/TiO2}$ = 0.1 g/L, C_0 = 10 mg/L and pH = 6.8)

phosphate ($H_2PO_4^-$), bicarbonate (HCO_3^-), and sulfate (SO_4^{2-}) anions all reduced the efficiency from 91.5% to 68.0%. The decrease in RhB removal efficiency was explained by the fact that these inorganic ions trap the photogenic holes (h^+) and free radicals $OH^•$. Since then, the photocatalytic efficiency of RhB has been reduced. In addition, inorganic anions can be adsorbed on the surface of the photocatalyst instead of the pollutant molecule, causing a decrease in the active sites of the photocatalyst and a decrease in the decolorization efficiency. Possible reactions in the presence of inorganic anions are illustrated by Eqs. (7)–(12) [15, 39].

$$Cl^- + h^+ \rightarrow Cl^• \tag{7}$$

$$Cl^• + Cl^- \rightarrow Cl_2^{•-} \tag{8}$$

$$Cl^- + OH^• \rightarrow Cl^• + OH^- \tag{9}$$

$$H_2PO_4^- + OH^• \rightarrow HPO_4^{•-} + H_2O \tag{10}$$

$$HCO_3^- + OH^• \rightarrow CO_3^{•-} + H_2O \tag{11}$$

$$SO_4^{2-} + OH^• \rightarrow SO_4^{•-} + OH^- \tag{12}$$

Butanol, Ethylene Diamine Tetra Acetic (EDTA), and Chloroform are organic substances used to investigate the effect of organic scavengers on RhB removal efficiency, and the results are shown in Fig. 15. Unlike inorganic anions, organic ions do not seem to interfere with the adsorption of RhB on the photocatalyst surface, so the decolorization efficiency decreased insignificantly from 91.5% to 80.2%. The chloroform molecules may have attacked the hydroxyl radicals, resulting in a reduced ability to generate hydroxyl radicals and subsequently decreased degradation efficiency. Meanwhile, butanol and EDTA in the
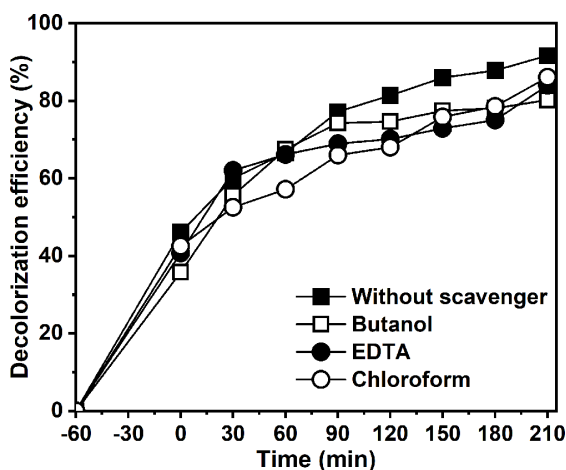
solution inhibited RhB degradation by scavenging photogenic holes (h^+), as illustrated in Eq. (13). Based on the above results, the RhB decolorization efficiency can be inhibited by the attack on free radicals by both organic and inorganic ion scavengers. Besides, the adsorption process also plays an important role in enhancing the photocatalytic degradation of RhB [45–47].

$$C_4H_9OH + h^+ \rightarrow C_4H_8O + 2H^+ \tag{13}$$

3.2.5 Rhodamine B photodegradation intermediates

The intermediate products after the photodegradation were identified by LC-MS analysis and presented in Fig. 16 with fifteen by-products corresponding to different m/z and denoted by (I) to (XV), where (I) is RhB ($m/z = 443$). Many publications have confirmed that during irradiation by a UVC source, the photoreaction occurs simultaneously and competitively between the N-demethylation and dye chromophore structure cleavage process. Next is the stage of the ring-opening process and mineralization [48–50]. Most N-demethylation process usually takes place by the formation of nitrogen-centered reactive radicals, one (or several) ethyl groups that cleave the xanthene ring in the RhB molecular structure, and by-products include N, N, N′−diethyl−N′−ethyl rhodamine ((II), $m/z = 415$); N, N−diethyl−rhodamine ((III), $m/z = 388$); N−ethyl−ethyl rhodamine ((IV), $m/z = 388$) [51]; N, N′−monomethyl−ethyl rhodamine ((V), $m/z = 360$) [52]; N, N′−ethyl rhodamine ((VI), $m/z = 332$) and N′−ethyl rhodamine ((VII), $m/z = 317$) [53]. Meanwhile, the dye chromophore structure cleavage process usually occurs by forming carbon-centered active radicals. Active species such as h^+, $^•OH$, and $^•O_2^-$ attack the carbon-centered in the RhB molecules and oxidize them to subsequent low-weight

Fig. 15 Effect of organic scavengers on the photocatalysis of RhB under UVC 15 W ($m_{MMT/TiO2}$ = 0.1 g/L, C_0 = 10 mg/L and pH = 6.8)
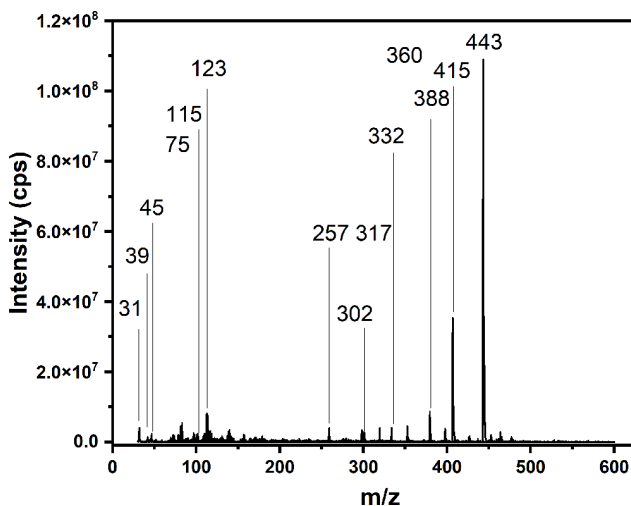

Fig. 16 The LC−MS spectrum of degradation products

by-products, including 2−(3H−xanthen−9−yl) benzoic acid ((VIII), $m/z = 302$); 9−phenyl−3H−xanthene ((IX), $m/z = 257$) and benzoic acid ((X), $m/z = 123$) [50, 52, 54]. The ring-opening process then occurs and forms small and broken-ring compounds, including malonic acid ((XI), $m/z = 115$); propane−1,2,3−triol ((XII), $m/z = 75$); oxalic acid ((XIII), $m/z = 45$); succinic acid ((XIV), $m/z = 39$) and ethane−1,2−diol ((XV), $m/z = 31$). Finally, these broken-ring compounds are completely mineralized to CO_2 and H_2O [55].

3.2.6 Kinetics model

0.1 g/L MMT, TiO_2 and MMT/TiO_2 were added to 100 mL of RhB 10 mg/L and pH = 6.8, respectively. Before irradiation for 210 min, the samples were stirred in the dark for 60 min to reach equilibration. The RhB removal efficiency of these samples over time is shown in Fig. 17 and summarized in Table 2. The results show that MMT has the highest adsorption efficiency (50.4%), while TiO_2 shows almost no adsorption properties (6.5%). MMT/TiO_2 has an adsorption efficiency of 46.3%, lower than that of MMT. This may be due to the TiO_2 particles intercalating between the clay layers and reducing the basal spacing of the MMT, leading to a decrease in the adsorption efficiency. When the RhB solution was exposed for 210 min
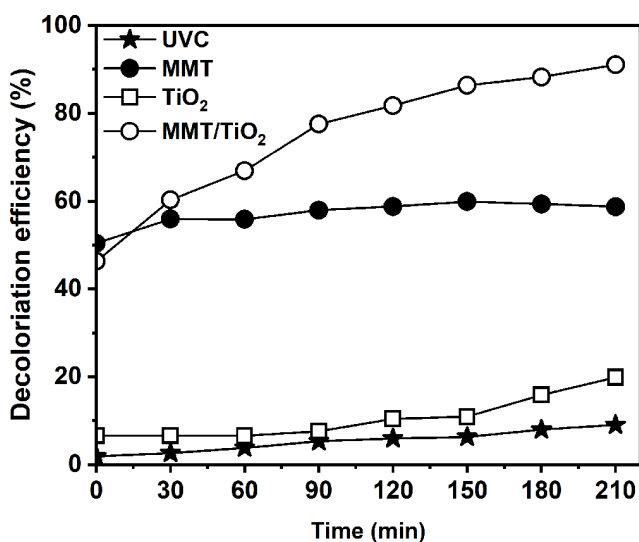

Fig. 17 The photocatalytic performance of MMT, TiO_2, and MMT/TiO_2 for RhB degradation under UVC 15 W and pH = 6.8

under UVC radiation (without the addition of a photocatalyst), the RhB removal efficiency was only less than 10%. This suggests that if only irradiation of a 15 W UVC lamp is present, there is not enough decomposition of the RhB solution. Notably, the photocatalytic activity under UVC irradiation of MMT and TiO_2 increased slightly (8.3% and 13.4%, respectively), while that of MMT/TiO_2 was the highest (45.2%). Therefore, the total RhB removal efficiency of MMT/TiO_2 was highest (91.5%), indicating that the heterostructure based on MMT and TiO_2 enhanced the photocatalytic activity of TiO_2 based on the previous adsorption of MMT [34, 56]. RhB removal efficiency based on the photocatalysis of any photocatalyst can be affected by factors such as irradiation source, pH value, catalyst content, initial concentration of RhB, exposure time, etc. Table 3 [57–60] summarizes the comparison of the RhB photocatalytic efficiency of MMT/TiO_2 in this study with those of the literature. The results showed that MMT/TiO_2 had superior RhB removal efficiency, demonstrating that the combination of MMT and TiO_2 significantly enhanced the RhB removal efficiency based on photocatalysis.

Many previous studies have confirmed that the photocatalytic degradation of organic compounds can be analyzed according to the Langmuir-Hinshelwood apparent first-order kinetic equation (Eq. (14)) [61, 62]. This is a kinetic model of the photocatalyst reaction considering the adsorption of colored organic compounds onto the surface of the photocatalyst. The kinetic parameters of RhB degradation over time of MMT, TiO_2, and MMT/TiO_2 are summarized in Table 2. The linear correlation between $\ln(C_0/C)$ and time t with high regression coefficients R^2 ($0.966 - 0.986$), as shown in Fig. 18, suggests that the RhB photodegradation reaction is suitable for the Langmuir-Hinshelwood first-order kinetic model. The reaction rate constants (k_{app}) are 0.0079, 0.0070, and 0.0824, respectively, for MMT, TiO_2, and MMT/TiO_2. The k_{app} value of MMT/TiO_2 is the highest compared to that of MMT or TiO_2, which confirms the enhancement of RhB photocatalyst efficiency by immobilizing TiO_2 nanoparticles to the surface or space between MMT clay layers, leading to MMT/TiO_2 having the highest photodegradation efficiency.

Table 2 Adsorption efficiency, photocatalytic activity, total efficiency, kinetic equations, reaction rate constants (k), and regression coefficients (R^2) of photocatalytic degradation of RhB for MMT, TiO_2, and MMT/TiO_2

Samples	Adsorption efficiency (%)	Photocatalytic activity (%)	Total efficiency (%)	Kinetic equations	k_{app} (min^{-1})	R^2
MMT	50.4	8.3	58.7	$y = 0.0079x + 0.76534$	0.0079	0.966
TiO_2	6.5	13.4	19.9	$y = 0.0070x + 0.03881$	0.0070	0.979
MMT/TiO_2	46.3	45.2	91.5	$y = 0.0824x + 0.67043$	0.0824	0.986

Table 3 The photocatalytic performance of MMT/TiO$_2$ to rhodamine B degradation compared to previous studies

Catalyst	Irradiation power	Initial concentration of rhodamine B (mg/L)	Catalyst amount (mg/L)	Degradation (%)	Exposed time (min)	Ref.
MMT/TiO$_2$	UV-C lamp (15 W)	10	10	91.5	210	this study
TiO$_2$/MMT	Xe lamp (500 W)	10	150	90	120	[54]
SnO$_2$/MMT	Ultrasonic probe (68 W)	20	500	95	120	[57]
ZnO/MMT	UV-C lamp (10 W)	10	10	60	300	[26]
Au/TiO$_2$	Xe lamp (300 W)	10^{-5} mol/L	50 mg/50 mL	95	150	[58]
Pt/TiO$_2$	UV light and sunlight irradiation	3.10^{-5} mol/L	0.1 g/100 mL	92	120	[59]
AgO$_2$/TiO$_2$ nanotubes	Xe lamp (300 W)	10	20 mg/100 mL	94.7	80	[60]
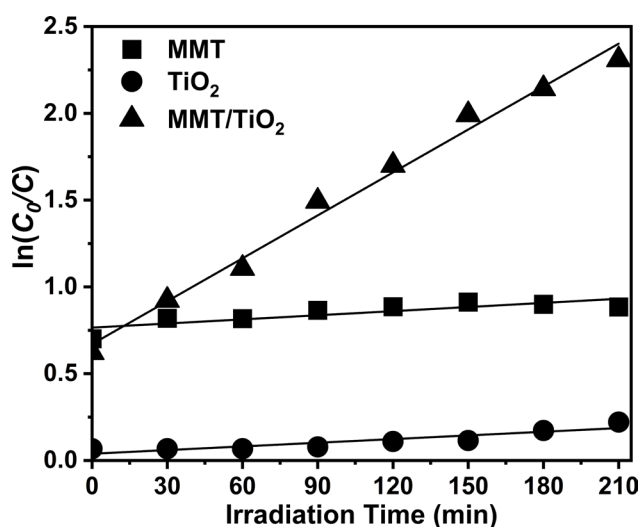
Fig. 18 Fitting curves of the kinetic model for MMT, TiO$_2$, and MMT/TiO$_2$

$$\ln \frac{C_0}{C} = k_{app}t \tag{14}$$

Equation (14) shows C_0: the concentration of the RhB initially (mg/L); C: the concentration of the RhB dyes at time t (mg/L); k_{app}: the apparent first order rate constant (min^{-1}); t: decomposition time (min).

4 Conclusion

The MMT/TiO$_2$ nanocomposite was synthesized as a heterogeneous photocatalyst using a simple wet stirring method with ultrasonication. Based on the structural characterization results, TiO$_2$ anatase nanoparticles have been successfully intercalated in MMT to form a nanocomposite with a house-of-card structure. As the matrix phase in composites, MMT offers positive advantages when both prevent the recombination of photogenerated electron-hole pairs and adsorbs organic dye molecules into active sites. Based on the photocatalytic test results, at pH 6.8 and after 210 min of exposure under a 15 W UVC source, 0.1 g/L MMT/TiO$_2$ removed 91.5% RhB 10 mg/L. Although RhB has not been fully mineralized, the final intermediate product, ethane−1,2−diol, showed the ability to cleave the chromophore structure and form small and broken-ring compounds by MMT/TiO$_2$. Based on the present results of this study, MMT/TiO$_2$ as a porous heterostructure is an effective photocatalyst for the removal of RhB or other similar dyes that are difficult to biodegrade in the textile wastewater industry.

References

[1] Cerrato, E., Gaggero, E., Calza, P., Paganini, M. C. "The role of Cerium, Europium and Erbium doped TiO$_2$ photocatalysts in water treatment: A mini-review", Chemical Engineering Journal Advances, 10, 100268, 2022.
https://doi.org/10.1016/j.ceja.2022.100268

[2] Idris, N. H. M., Cheong, K. Y., Kennedy, B. J., Ohno, T., Lee, H. L. "Buoyant titanium dioxide (TiO$_2$) as high performance photocatalyst and peroxide activator: A critical review on fabrication, mechanism and application", Journal of Environmental Chemical Engineering 10(3), 107549, 2022.
https://doi.org/10.1016/j.jece.2022.107549

[3] Chen, D., Cheng, Y., Zhou, N., Chen, P., Wang, Y., Li, K., Huo, S., Cheng, P., Peng, P., Zhang, R., Wang, L., Liu, H., Liu, Y., Ruan, R. "Photocatalytic degradation of organic pollutants using TiO_2-based photocatalysts: A review", Journal of Cleaner Production, 268, 121725, 2020.
https://doi.org/10.1016/j.jclepro.2020.121725

[4] Do, H. H., Nguyen, D. L. T., Nguyen, X. C., Le, T.-H., Nguyen, T. P., Trinh, Q. T., Ahn, S. H., Vo, D.-V. N., Kim, S. Y., Le, Q. V. "Recent progress in TiO_2-based photocatalysts for hydrogen evolution reaction: A review", Arabian Journal of Chemistry, 13(2), pp. 3653–3671, 2020.
https://doi.org/10.1016/j.arabjc.2019.12.012

[5] Nur, A. S. M., Sultana, M., Mondal, A., Islam, S., Robel, F. N., Islam, A., Sumi, M. S. A. "A review on the development of elemental and codoped TiO_2 photocatalysts for enhanced dye degradation under UV–vis irradiation", Journal of Water Process Engineering, 47, 102728, 2022.
https://doi.org/10.1016/j.jwpe.2022.102728

[6] Mottola, S., Mancuso, A., Sacco, O., De Marco, I., Vaiano, V. "Production of hybrid TiO_2/β-CD photocatalysts by supercritical antisolvent micronization for UV light-driven degradation of azo dyes", The Journal of Supercritical Fluids, 188, 105695, 2022.
https://doi.org/10.1016/j.supflu.2022.105695

[7] Sridevi, A., Ramji, B. R., Prasanna Venkatesan, G. K. D., Sugumaran, V., Selvakumar, P. "A facile synthesis of $TiO_2/BiOCl$ and $TiO_2/BiOCl/La_2O_3$ heterostructure photocatalyst for enhanced charge separation efficiency with improved UV-light catalytic activity towards Rhodamine B and Reactive Yellow 86", Inorganic Chemistry Communications, 130, 108715, 2021.
https://doi.org/10.1016/j.inoche.2021.108715

[8] Zhang, Z., Chen, X., Chen, S., Dong, Q., Zhang, X., Jiang, A., Zhang, D., Di, Y., Li, T. "Synergistic interaction of Z-scheme TiO_2/g-C_3N_4 photocatalyst and peroxymonosulfate for improving the photocatalytic efficiency of Rhodamine B", Optical Materials, 133, 113081, 2022.
https://doi.org/10.1016/j.optmat.2022.113081

[9] Zhang, L., Guo, J., Hao, B., Ma, H. "WO_3/TiO_2 heterojunction photocatalyst prepared by reactive magnetron sputtering for Rhodamine B dye degradation", Optical Materials 133, 113035, 2022.
https://doi.org/10.1016/j.optmat.2022.113035

[10] Thuc, C.-N. H., Grillet, A.-C., Reinert, L., Ohashi, F., Thuc, H. H., Duclaux, L. "Separation and purification of montmorillonite and polyethylene oxide modified montmorillonite from Vietnamese bentonites", Applied Clay Science, 49(3), pp. 229–238, 2010.
https://doi.org/10.1016/j.clay.2010.05.011

[11] Dao, T. B. T., Ha, T. T. L., Nguyen, T. D., Le, H. N., Ha-Thuc, C. N., Nguyen, T. M. L., Perre, P., Nguyen, D. M. "Effectiveness of photocatalysis of MMT-supported TiO_2 and TiO_2 nanotubes for rhodamine B degradation", Chemosphere, 280, 130802, 2021.
https://doi.org/10.1016/j.chemosphere.2021.130802

[12] Yılmazoğlu, M., Turana, B., Demircivi, P., Hızal, J. "Synthesis and characterization of imidazolium based ionic liquid modified montmorillonite for the adsorption of Orange II dye: Effect of chain length", Journal of Molecular Structure, 1249, 131628, 2022.
https://doi.org/10.1016/j.molstruc.2021.131628

[13] Al Kausor, M., Sen Gupta, S., Bhattacharyya, K. G., Chakrabortty, D. "Montmorillonite and modified montmorillonite as adsorbents for removal of water soluble organic dyes: A review on current status of the art", Inorganic Chemistry Communications, 143, 109686, 2022.
https://doi.org/10.1016/j.inoche.2022.109686

[14] Hassani, A., Khataee, A., Karaca, S. "Photocatalytic degradation of ciprofloxacin by synthesized TiO_2 nanoparticles on montmorillonite: Effect of operation parameters and artificial neural network modeling", Journal of Molecular Catalysis A: Chemical, 409, pp. 149–161, 2015.
https://doi.org/10.1016/j.molcata.2015.08.020

[15] Khataee, A., Kiransan, M., Karaca, S., Arefi-Oskoui, S. "Preparation and characterization of ZnO/MMT nanocomposite for photocatalytic ozonation of a disperse dye", Turkish Journal of Chemistry, 40(4), pp. 546–564, 2016.
http://doi.org/10.3906/kim-1507-77

[16] Hassani, A., Khataee, A., Karaca, S., Karaca, C., Gholami, P. "Sonocatalytic degradation of ciprofloxacin using synthesized TiO_2 nanoparticles on montmorillonite", Ultrasonics Sonochemistry, 35(A), pp. 251–262, 2017.
http://doi.org/10.1016/j.ultsonch.2016.09.027

[17] Bessekhouad, Y., Robert, D., Weber, J.-V., Chaoui, N. "Effect of alkaline-doped TiO_2 on photocatalytic efficiency", Journal of Photochemistry and Photobiology A: Chemistry, 167(1), pp. 49–57, 2004.
http://doi.org/10.1016/j.jphotochem.2003.12.001

[18] Bakar, M., Kucharczyk, W., Stawarz, S., Żurowski, W. "Effect of nanopowders (TiO_2 and MMT) and aramid honeycomb core on ablative, thermal and dynamic mechanical properties of epoxy composites", Composite Structures, 259, 113450, 2021.
https://doi.org/10.1016/j.compstruct.2020.113450

[19] Gulen, B., Demircivi, P. "Synthesis and characterization of montmorillonite/ciprofloxacin/TiO_2 porous structure for controlled drug release of ciprofloxacin tablet with oral administration", Applied Clay Science, 197, 105768, 2020.
https://doi.org/10.1016/j.clay.2020.105768

[20] Liao, M., Liu, Z., Gao, Y., Liu, L., Xiang, S. "Study on UV aging resistance of nano-TiO_2/montmorillonite/styrene-butadiene rubber composite modified asphalt based on rheological and microscopic properties", Construction and Building Materials, 301, 124108, 2021.
https://doi.org/10.1016/j.conbuildmat.2021.124108

[21] Peña-Parás, L., Rodríguez-Villalobos, M., Maldonado-Cortés, D., Guajardo, M., Rico-Medina, C. S., Elizondo, G., Quintanilla, D. I. "Study of hybrid nanofluids of TiO_2 and montmorillonite clay nanoparticles for milling of AISI 4340 steel", Wear, 477, 203805, 2021.
https://doi.org/10.1016/j.wear.2021.203805

[22] Malika, M., Sonawane, S. S. "Statistical modelling for the Ultrasonic photodegradation of Rhodamine B dye using aqueous based Bi-metal doped TiO_2 supported montmorillonite hybrid nanofluid via RSM", Sustainable Energy Technologies and Assessments, 44, 100980, 2021.
https://doi.org/10.1016/j.seta.2020.100980

[23] Zhang, G. K., Ding, X. M., He, F. S., Yu, X. Y., Zhou, J., Hu, Y. J., Xie, J. W. "Low-Temperature Synthesis and Photocatalytic Activity of TiO$_2$ Pillared Montmorillonite", Langmuir, 24(3), pp. 1026–1030, 2008.
https://doi.org/10.1021/la702649v

[24] Kim, D., Mittal, G., Kim, M., Kim, S., Rhee, K. Y. "Surface modification of MMT and its effect on fatigue and fracture behavior of basalt/epoxy based composites in a seawater environment", Applied Surface Science, 473, pp. 55–58, 2019.
https://doi.org/10.1016/j.apsusc.2018.12.127

[25] Ullah, N., Ali, Z., Ullah, S., Khan, A. S., Adalat, B., Nasrullah, A., Alsaadi, M., Ahmad, Z. "Synthesis of activated carbon-surfactant modified montmorillonite clay-alginate composite membrane for methylene blue adsorption", Chemosphere, 309(1), 136623, 2022.
https://doi.org/10.1016/j.chemosphere.2022.136623

[26] Pannak, P., Songsasen, A., Foytong, W., Kidkhunthod, P., Sirisaksoontorn, W. "Homogeneuos distribution of nanosized ZnO in montmorillonite clay sheets for the photocatalytic enhancement in degradation of Rhodamine B", Research on Chemical Intermediates, 44(11), pp. 6861–6875, 2018.
https://doi.org/10.1007/s11164-018-3526-6

[27] Umer, M., Tahir, M., Azam, M. U., Tahir, B., Jaffar, M. M., Alias, H. "Montmorillonite dispersed single wall carbon nanotubes (SWCNTs)/TiO$_2$ heterojunction composite for enhanced dynamic photocatalytic H$_2$ production under visible light", Applied Clay Science, 174, pp. 110–119, 2019.
https://doi.org/10.1016/j.clay.2019.03.029

[28] Bahranowski, K., Gaweł, A., Klimek, A., Michalik-Zym, A., Napruszewska, B. D., Nattich-Rak, M., Rogowska, M., Serwicka, E. M. "Influence of purification method of Na-montmorillonite on textural properties of clay mineral composites with TiO$_2$ nanoparticles", Applied Clay Science, 140, pp. 75–80, 2017.
https://doi.org/10.1016/j.clay.2017.01.032

[29] Liang, H., Wang, Z., Liao, L., Chen, L., Li, Z., Feng, J. "High performance photocatalysts: Montmorillonite supported-nano TiO$_2$ composites", Optik, 136, pp. 44–51, 2017.
https://doi.org/10.1016/j.ijleo.2017.02.018

[30] Xiang, H., Tuo, B., Tian, J., Hu, K., Wang, J., Cheng, J., Tang, J. "Preparation and photocatalytic properties of Bi-doped TiO$_2$/montmorillonite composite", Optical Materials, 117, 111137, 2021.
https://doi.org/10.1016/j.optmat.2021.111137

[31] Chen, J. D., Liao, W. S., Jiang, Y., Yu, D. N., Zou, M. L., Zhu, H., Zhang, M., Du, M. L. "Facile Fabrication of ZnO/TiO$_2$ Heterogeneous Nanofibres and Their Photocatalytic Behaviour and Mechanism towards Rhodamine B", Nanomaterials and Nanotechnology, 6, 62291, 2016.
https://doi.org/10.5772/62291

[32] Umer, M., Tahir, M., Azam, M. U., Jaffar, M. M. "Metal free MWCNTs@TiO$_2$@MMT heterojunction composite with MMT as a mediator for fast charges separation towards visible light driven photocatalytic hydrogen evolution", Applied Surface Science, 463, pp. 747–757, 2018.
https://doi.org/10.1016/j.apsusc.2018.08.240

[33] Miao, S., Liu, Z., Han, B., Zhang, J., Yu, X., Du, J., Sun, Z. "Synthesis and characterization of TiO$_2$–montmorillonite nanocomposites and their application for removal of methylene blue", Journal of Materials Chemistry, 16(6), pp. 579–584, 2006.
https://doi.org/10.1039/B511426H

[34] Mishra, A., Sharma, M., Mehta, A., Basu, S. "Microwave Treated Bentonite Clay Based TiO$_2$ Composites: An Efficient Photocatalyst for Rapid Degradation of Methylene Blue", Journal of Nanoscience and Nanotechnology, 17(2), pp. 1149–1155, 2017.
https://doi.org/10.1166/jnn.2017.12674

[35] Ooka, C., Yoshida, H., Suzuki, K., Hattori, T. "Effect of surface hydrophobicity of TiO$_2$-pillared clay on adsorption and photocatalysis of gaseous molecules in air", Applied Catalysis A: General, 260(1), pp. 47–53, 2004.
https://doi.org/10.1016/j.apcata.2003.10.001

[36] Khataee, A., Sheydaei, M., Hassani, A., Taseidifar, M., Karaca, S. "Sonocatalytic removal of an organic dye using TiO$_2$/Montmorillonite nanocomposite", Ultrasonics Sonochemistry, 22, pp. 404–411, 2015.
https://doi.org/10.1016/j.ultsonch.2014.07.002

[37] Chen, F., Zhao, E., Kim, T., Wang, J., Hableel, G., Reardon, P. J. T., Ananthakrishna, S. J., Wang, T., Arconada-Alvarez, S., Knowles, J. C., Jokerst, J. V. "Organosilica Nanoparticles with an Intrinsic Secondary Amine: An Efficient and Reusable Adsorbent for Dyes", ACS Applied Materials and Interfaces, 9(18), pp. 15566–15576, 2017.
https://doi.org/10.1021/acsami.7b04181

[38] Surenjan, A., Sambandam, B., Pradeep, T., Philip, L. "Synthesis, characterization and performance of visible light active C-TiO$_2$ for pharmaceutical photodegradation", Journal of Environmental Chemical Engineering, 5(1), pp. 757–767, 2017.
https://doi.org/10.1016/j.jece.2016.12.044

[39] Karaca, M., Kıranssan, M., Karaca, S., Khataee, A., Karimi, A. "Sonocatalytic removal of naproxen by synthesized zinc oxide nanoparticles on montmorillonite", Ultrasonics Sonochemistry, 31, pp. 250–256, 2016.
http://doi.org/10.1016/j.ultsonch.2016.01.009

[40] Djellabi, R., Ghorab, M. F., Cerrato, G., Morandi, S., Gatto, S., Oldani, V., Di Michele, A., Bianchi, C. L. "Photoactive TiO$_2$–montmorillonite composite for degradation of organic dyes in water", Journal of Photochemistry and Photobiology A: Chemistry, 295, pp. 57–63, 2014.
https://doi.org/10.1016/j.jphotochem.2014.08.017

[41] Heidari, A., Shahbazi, A., Aminabhavi, T. M., Barceló, D., Rtimi, S. "A systematic review of clay-based photocatalysts for emergent micropollutants removal and microbial inactivation from aqueous media: Status and limitations", Journal of Environmental Chemical Engineering, 10(6), 108813, 2022.
https://doi.org/10.1016/j.jece.2022.108813

[42] Hassani, A., Khataee, A., Karaca, S., Fathinia, M. "Degradation of mixture of three pharmaceuticals by photocatalytic ozonation in the presence of TiO$_2$/montmorillonite nanocomposite: Simultaneous determination and intermediates identification", Journal of Environmental Chemical Engineering, 5(2), pp. 1964–1976, 2017.
https://doi.org/10.1016/j.jece.2017.03.032

[43] Krishnakumar, B., Swaminathan, M. "Influence of operational parameters on photocatalytic degradation of a genotoxic azo dye Acid Violet 7 in aqueous ZnO suspensions", Spectrochimica Acta Part A: Molecular and Biomolecular Spectroscopy, 81(1), pp. 739–744, 2011.
https://doi.org/10.1016/j.saa.2011.07.019

[44] Yetim, T., Tekin, T. "A kinetic study on photocatalytic and sono-photocatalytic degradation of textile dyes", Periodica Polytechnica Chemical Engineering, 61(2), pp. 102–108, 2017.
https://doi.org/10.3311/PPch.8535

[45] Ghanbari, F., Zirrahi, F., Olfati, D., Gohari, F., Hassani, A. "TiO$_2$ nanoparticles removal by electrocoagulation using iron electrodes: Catalytic activity of electrochemical sludge for the degradation of emerging pollutants", Journal of Molecular Liquids, 310, 113217, 2020.
https://doi.org/10.1016/j.molliq.2020.113217

[46] Asgari, E., Sheikhmohammadi, A., Nourmoradi, H., Nazari, S, Aghanaghad, M. "Degradation of ciprofloxacin by photocatalytic ozonation process under irradiation with UVA: Comparative study, performance and mechanism", Process Safety and Environmental Protection, 147, pp. 356–366, 2021.
https://doi.org/10.1016/j.psep.2020.09.041

[47] Ateia, M., Alalm, M. G., Awfa, D., Johnson, M. S., Yoshimura, C. "Modeling the degradation and disinfection of water pollutants by photocatalysts and composites: A critical review", Science of The Total Environment, 698, 134197, 2020.
https://doi.org/10.1016/j.scitotenv.2019.134197

[48] Kashyap, J., Ashraf, S. M., Riaz, U. "Highly Efficient Photocatalytic Degradation of Amido Black 10B Dye Using Polycarbazole-Decorated TiO$_2$ Nanohybrids", ACS Omega, 2(11), pp. 8354–8365, 2017.
https://doi.org/10.1021/acsomega.7b01154

[49] Guo, N., Fu, Y., Hu, J. S. "Preparation of Fe$_2$O$_3$ nanoparticles doped with In$_2$O$_3$ and photocatalytic degradation property for rhodamine B", Optik, 201, pp. 1635–1637, 2020.
https://doi.org/10.1016/j.ijleo.2019.163537

[50] Wermuth, T. B., Arcaro, S., Venturini, J., Ribeiro, T. M. H., Rodriguez, A. A. L., Machado, E. L., Oliveira, T. F., Oliveira, S. E. F., Baibich, M. N., Bergmann, C. P. "Microwave-synthesized KNbO$_3$ perovskites: photocatalytic pathway on the degradation of rhodamine B", Ceramics International, 45(18), pp. 24137–24145, 2020.
https://doi.org/10.1016/j.ceramint.2019.08.122

[51] Xiao, C., Tan, Z., Wang, C., Yang, X., Zhang, G., Pan, H. "Fabrication of In$_2$O$_3$/TiO$_2$ nanotube arrays hybrids with homogeneously developed nanostructure for photocatalytic degradation of Rhodamine B", Materials Research Bulletin, 106, pp. 197–203, 2018.
https://doi.org/10.1016/j.materresbull.2018.05.022

[52] Hegazey, R. M., Abdelrahman, E. A., Kotp, Y. H. "Facile fabrication of hematite nanoparticles from Egyptian insecticide cans for efficient photocatalytic degradation of rhodamine B dye", Journal of Materials Research and Technology, 9(2), pp. 1652–1661, 2020.
https://doi.org/10.1016/j.jmrt.2019.11.090

[53] Sharmaa, G., Dionysiou, D. D., Sharm, S., Kumar, A., Al-Muhtaseb, A. H., Naushad, M., Stadler, F. J. "Highly efficient Sr/Ce/activated carbon bimetallic nanocomposite for photoinduced degradation of rhodamine B", Catalysis Today, 335, pp. 437–451, 2019.
https://doi.org/10.1016/j.cattod.2019.03.063

[54] Tao, E., Xiao, X., Yang, S. "A new synthesizing method of TiO$_2$ with montmorillonite: effective photoelectron transfer to degrade Rhodamine B", Separation and Purification Technology, 258(2), 118070, 2021.
https://doi.org/10.1016/j.seppur.2020.118070

[55] Isari, A. A., Payan, A., Fattahi, M., Jorfi, S., Kakavandi, B. "Photocatalytic degradation of Rhodamine B and Real Textile Wastewater using Fe-Doped TiO$_2$ anchored on Reduced Graphene Oxide (Fe-TiO$_2$/rGO): Characterization and feasibility, mechanism and pathway studies", Applied Surface Science, 462, pp. 549–564, 2018.
https://doi.org/10.1016/j.apsusc.2018.08.133

[56] Kang, S.-Z., Wu, T., Li, X., Mu, J. "Effect of montmorillonite on the photocatalytic activity of TiO$_2$ nanoparticles", Desalination, 262(1–3), pp. 147–151, 2010.
https://doi.org/10.1016/j.desal.2010.06.003

[57] Fatimah, I., Nurillahi, R., Sahroni, I., Fadillah, G., Nugroho, B. H., Kamari, A., Murazad, O. "Sonocatalytic degradation of rhodamine B using tin oxide/ montmorillonite", Journal of Water Process Engineering, 37, 101418, 2020.
https://doi.org/10.1016/j.jwpe.2020.101418

[58] Chen, L., Tian, L., Zhao, X., Hu, Z., Fan, J., Lv, K. "SPR effect of Au nanoparticles on the visible photocatalytic RhB degradation and NO oxidation over TiO$_2$ hollow nanoboxes", Arabian Journal of Chemistry, 13(2), pp. 4404–4416, 2020.
https://doi.org/10.1016/j.arabjc.2019.08.011

[59] Abdel-Khalek, M. H., Ahmed, M. A., Abdel-Messih, M. F., El-Shahat, F. "Synthesis of mesoporous Pt/TiO$_2$ nanoparticles by incipient wetness route for photocatalytic degradation of rhodamine B and methyl orange dyes under UV and sunlight radiations", Materials Science for Energy Technologies, 5, pp. 334–343, 2022.
https://doi.org/10.1016/j.mset.2022.08.001

[60] Gao, Y., Wang, T. "Preparation of Ag$_2$O/TiO$_2$ nanocomposites by two-step method and study of its degradation of RHB", Journal of Molecular Structure, 1224, 129049, 2021.
https://doi.org/10.1016/j.molstruc.2020.129049

[61] Sani, H. A., Ahmad, M. B., Hussein, M. Z., Ibrahim, N. A., Musa, A., Saleh, T. A. "Nanocomposite of ZnO with Montmorillonite for Removal of Lead and Copper Ions from aqueous solutions", Process Safety and Environment Protection, 109, pp. 97–105, 2017.
http://doi.org/10.1016/j.psep.2017.03.024

[62] Hosseini, A., Karimi, H., Foroughi, J., Sabzehmeidani, M. M., Ghaedi, M. "Heterogeneous photoelectro-Fenton using ZnO and TiO$_2$ thin film as photocatalyst for photocatalytic degradation Malachite Green", Applied Surface Science Advances, 6, 100126, 2021.
https://doi.org/10.1016/j.apsadv.2021.100126